SDO/AIA Observation of Kelvin-Helmholtz Instability in the Solar Corona

L. Ofman[1,2,3] and B. J. Thompson[2]

[1]Catholic University of America, Washington, DC 20064

[2]NASA Goddard Space Flight Center, Code 671, Greenbelt, MD 20771

[2]Visiting, Department of Geophysics and Planetary Sciences, Tel Aviv University, Tel Aviv, Israel

ABSTRACT

We present observations of the formation, propagation and decay of vortex-shaped features in coronal images from the Solar Dynamics Observatory (SDO) associated with an eruption starting at about 2:30UT on Apr 8, 2010. The series of vortices formed along the interface between an erupting (dimming) region and the surrounding corona. They ranged in size from several to ten arcseconds, and traveled along the interface at 6-14 km s^{-1}. The features were clearly visible in six out of the seven different EUV wavebands of the Atmospheric Imaging Assembly (AIA). Based on the structure, formation, propagation and decay of these features, we identified the event as the first observation of the Kelvin-Helmholtz (KH) instability in the corona in EUV. The interpretation is supported by linear analysis and by MHD model of KH instability. We conclude that the instability is driven by the velocity shear between the erupting and closed magnetic field of the Coronal Mass Ejection (CME). The shear flow driven instability can play an important role in energy transfer processes in coronal plasma.

Subject headings: Sun: activity Sun: corona Sun: coronal mass ejections (CMEs)
Sun: UV radiation: instabilities: magnetohydrodynamics (MHD)

1.   Introduction

The Kelvin-Helmholtz (KH) instability, produced by two fluids undergoing differential shearing motion across an interface, was described by Kelvin (1871) and Helmholtz (1868) almost one and a half centuries ago. The KH instability is observed over a wide range of gaseous, fluid, and plasma regimes on the Earth and in space. Chains of vortex-shaped features have been observed in clouds on the Earth, and in the atmospheric cloud belts of Jupiter and Saturn that exhibit shearing wind motions. These vortices were interpreted as signatures of the KH instability. KH vortices have been observed in the Earth's aurora (Farrugia et al. 1994) and the magnetosphere, where there is evidence that the instability plays an important role in the energy transport of solar wind into the magnetosphere (Hasegawa et al. 2004). Observations have also been made in the magnetospheres of Mercury (Slavin et al. 2010), Saturn (Masters et al. 2010), and Ganymede (Kivelson et al. 1998). Recently, evidence of KH development in solar prominence material was found in observations from the Hinode Solar Optical Telescope (Ryutova et al. 2010; Berger et al. 2010).

The growth rate of the instability was calculated analytically for sheared flow in an idealized fluid (Chandrasekhar 1961). This instability can also occur in magnetized plasma of the solar corona; in this case the magnetic field component along the direction of the shear can have a stabilizing effect (Chandrasekhar 1961) and can also affect the growth rate and structure of the vortices (Lysak & Song 1996).Non-uniform (sheared) magnetic field across the velocity shear layer can have stabilizing or destabilizing effect on the KH mode, depending on the properties of the magnetic shear (e.g., Ofman et al. 1991). The KH instability has been studied theoretically in the context of coronal plasmas, where it is believed to play an important role in the transition to turbulence and plasma heating (Heyvaerts & Priest 1983; Ofman et al. 1994; Karpen et al. 1994).KH instability was also

proposed as a mechanism that produces the observed quasi-periodic pulsation in flare high energy emission (Ofman & Sui 2006). In this study we report the first observation of KH instability in the solar corona in EUV coronal lines by SDO/AIA. The interpretation of observations is supported by linear analysis and MHD model of KH instability. The paper is organized as follows: § 2 is devoted to the description of SDO/AIA observations, § 3 described briefly the theory of KH instability, § 4 is devoted to numerical result of MHD model, and the conclusion are in § 5.

2. Observations

The Atmospheric Imaging Assembly (AIA) on SDO is an array of four telescopes that captures images of the Sun's atmosphere out to $1.3R_\odot$ in ten separate wave bands. Seven of the ten channels are centered on EUV wavelengths: 94Å (Fe XVIII), 131Å (Fe VIII, XX, XXIII), 171Å (Fe IX), 193Å (FeXII, XXIV), 211Å (Fe XIV), 304Å (He II) and 335Å (Fe XVI), representing a range of effective temperatures from the upper chromosphere to the corona. The images are 4096×4096 square with a pixel width of 0.6″.

SDO was launched on 11 February 2010, and on 8 April 2010 the observatory was still undergoing its post-launch commissioning phase. AIA was taking a full set of images every 20 seconds in preparation for the transition to nominal science operations which would have a 10- to 12-second cadence. On 8 April 2010 beginning at 02:34 UT, AIA observed a flare and coronal mass ejection coming from an active region located 16° E and 29° N of heliographic disk center. The flare peaked at 03:25 UT at a flux of B3.7 on the GOES magnitude scale, and STEREO SECCHI measured the CME's speed to be around 500 km s^{-1}. In addition to the flare, the primary indicator of the CME in the AIA images was the formation of large-scale dimming regions adjacent to the active region (see Figure 1). These dimming regions are the site of plasma evacuated by the eruption.

Along the boundary of one of the dimming regions, we identify the formation, propagation and decay of vortex-shaped features ranging from several to ten arcseconds in size. They traveled at speeds ranging from $\sim 6 - 14$ km s^{-1} along the boundary, which we identify as the shearing interface between erupting magnetic fields and the surrounding, non-erupting corona. Based on the structure, evolution and decay of these features and supported by theoretical results (see below), we believe that these are the first observations of the Kelvin- Helmholtz instability in the corona in EUV.

The vortex-shaped features are clearly visible in six of AIA's EUV wavebands, and are partially visible in the 94Å images. The corona imaged in the 94Å is the hottest of the AIA wavebands (around 6 MK), while the plasma at the dimming boundary is closer to typical coronal temperatures of 1-2MK. The observed vortices are small (~ 7000 km) and evolve rapidly, disappearing on timescales of tens of minutes. In Figure 1 we show the solar disk observed in the EUV 171Å waveband. The outer box shows the location of the CME eruption, while the inner box shows the boundary of the dimming region where the vortices were observed. In the right panel we highlight the evolution of the vortices in a sampling of 211Å images ranging from t = 3:20:53 UT to t = 3:37:53 UT (see the accompanying animations of this event). The vortices propagate from right to left at speeds ranged from $\sim 6 - 14$ km s^{-1}. All in all, aspects of these vortices were visible for more than an hour.

The first sign of vortex formation is at 3:00:13UT, and the flow of the vortices along the boundary was fully developed by 3:13:13UT. The vortex and associated features lasted until about 4:47:13UT. In order to study the motion of the vortices in Figure 2 we show the interface boundary stacked in time, where the x-axis is the location across the solar coordinate in arcseconds, and the y-axis is time in seconds (lower panel). Cuts were taken from a total of 51 images in 211Å from a period of 3:20UT to 3:40UT, which corresponds to the period in which the vortex motion was most visible. The average difference between

consecutive images was 20-25 seconds. In order to obtain the speed relative to the curved interface the stacks are shown along the coordinate of the interface s on the x-axis, and time on the y-axis. The dashed lines in the figure indicate slopes corresponding to speeds of 6 km s^{-1} and 14 km s^{-1}, after compensating for the velocity of solar rotation.

The motion of the magnetic loops associated with the erupting CME on April 8, 2010 are shown in Figure 3. The five frames show difference images that were created from consecutive pairs of 211Å images taken at $t =$2:51:13, 2:55:13, 3:00:33, 3:08:33, and 3:13:55UT. The AIA image of the region at 3:13:53UT is shown for context. The difference images enhance the structure and the evolution of the loops. We have estimated the upper limit of the speed of the shearing field motion in the initial stages of the eruption by tracking several loop features as a function of time, and found that their velocity was $\sim$ 20 km s^{-1}. We assume that this velocity is close to the velocity at which the material is evacuated from the dark regions, and that the projection effects are small. Thus, we can estimate the relative velocity between the non-erupting (stationary), and erupting region. By observing the width of the interface between the two regions before the formation of the vortices we estimate the thickness of the interface as 1-3 pixels. Thus, on average the interface is $\sim$800 km thick, and the velocity must change from zero to $\sim$ 20 km s^{-1} over this thickness. This is the initial driving shear of the KH instability (see below).

The first indication of the appearance of the dimming structure is around 2:42:53UT, and it's fairly well defined by 2:51:13UT. The dimming structure expands and reaches the location where the KH vortices eventually develop. The first image where we see any motion along the KH front is 3:13:53UT. Thus, we can roughly estimate that the growth time of the KH instability to the nonlinear stage is on the order of 14 minutes.

3. Kelvin-Helmholtz instability

The KH instability in fluids or plasmas arise when there is a velocity discontinuity or finite thickness velocity shear over an interface between two regions (Kelvin 1871; Helmholtz 1868; Chandrasekhar 1961) , and it is observed in many natural phenomena as well as in laboratory fluids or plsamas. In the initial linear stage the KH instability exhibits exponential growth, followed by nonlinear saturation and the formation of the typical KH vortices on the interface between the fluids, thus broadening the interface and reducing the magnitude of the shear. The kinetic energy of the shear is converted to the kinetic energy of the vortices that further transport it to smaller scales. In magnetized plasma the orientation of the magnetic field has an important role on the growth of the KH instability (Chandrasekhar 1961). When the magnetic field has significant component parallel to the interface, the growth of the KH instability can be suppressed. The strength of the magnetic field affects the size and the complexity of the vortices produced by KH instability in magnetized plasma. The linear growth rate of KH instability in an incompressible fluid with a discontinuous velocity jump between the two regions is (Chandrasekhar 1961; Frank et al. 1996)

$$\gamma = \frac{1}{2}|\mathbf{k} \cdot \Delta \mathbf{V}|[1 - (2V_A\hat{\mathbf{k}} \cdot \hat{\mathbf{B}})^2/(\hat{\mathbf{k}} \cdot \Delta \mathbf{V})^2]^{1/2}, \tag{1}$$

where $\Delta \mathbf{V}$ is the velocity jump over the interface, $\mathbf{B}$ is the magnetic field, k is the wavevector, $V_A = B/\sqrt{4\pi\rho}$ is the Alfvén speed, and ρ is the density. When the interface region is of a finite width the growth rate is reduced compared to the case with discontinuous jump in velocity.

Based on the parameters of the observed velocity shear in the range 6-14 km s^{-1}, wavelength of 7000 km (based on the size of the initial ripples), and assuming that the velocity jump is discontinuous since it is much smaller than the wavelength, we can estimate the upper limit of the linear growth rate of the KH instability using the above equation:

$\gamma_{KH} \approx 0.003 - 0.006$ s^{-1}. For simplicity, we have assumed that the magnetic field has no parallel component to the interface in Equation 1. The nonlinear saturation is reached at time scale of several γ^{-1} or in about 10 minutes, is in agreement with the observed time scale of the evolution. We relax some of the simplifying assumptions in the MHD model. Note that the KH instability is not strongly suppressed, implying that the magnetic field was mostly radial (i.e., perpendicular to the plane of the velocity shear) at the interface. This is in agreement with the observations of the erupting loops, which stretch the magnetic field and evolve to a nearly radial orientation as the eruption proceeds.

4. Numerical Model

Here, we describe the results of numerical 2.5D (i.e., two spatial dimensions and 3 components of magnetic field and velocity) MHD model of KH instability as a simplified model the magnetic and velocity structures seen by AIA. Numerical studies have been developed in the past to model the behavior of KH instability in a magnetized plasma, with initial velocity shear and weak magnetic field in the plane of the shear using a 2.5D MHD model (e.g., Miura & Pritchett 1982; Miura 1984; Frank et al. 1996, and similar studies). Here, we solve the compressible resistive MHD equations in the 2D Cartesian $x - y$ plane, without gravity (since it is perpendicular to the plane), and isothermal energy equation (see, Ofman & Thompson 2002, for the description of the equations and the normalization) and with the following initial state (Figure 4):

$$V_{x0}(y) = (V_0/2)\tanh(y/a) \tag{2}$$

$$\rho_0(y) = \frac{1}{2}(\rho_{max} + \rho_{min}) - \frac{1}{2}(\rho_{max} - \rho_{min})\tanh(y/a), \tag{3}$$

where a is the width of the shear layer in V_{x0} and ρ_0, and the density is varied similarly between ρ_{max} and ρ_{min}, and $a = 800$ km, guided by AIA observations. In order to determine the density ratio between the bright and dark (evacuated) regions across the interface

we have examined the emission ratio in EUV AIA images for several wavebands. We found that the emission ratio is on average ~ 5 with a range of 3-10. Since the density is proportional to the emission square for the same column depth in the line of sight, we have used $\rho_{max}/\rho_{min} = 5^{1/2}$ in the model to represent the average observed value. We have also performed runs with density ratios of 2 and 3 and found similar results, with the growth rate of KH instability decreasing by $\sim 15\%$ with the density ratio in this range. The initial magnetic field is taken to be $\mathbf{B}_0 = B_{x0}\hat{x} + B_{z0}(y)\hat{z}$, with constant B_{x0}, and the form of $B_{z0}(y)$ determined from pressure balance over the interface, i.e., in normalized units $B_{z0}(y)^2/2 + \beta\rho_0(y) = const$. Since we assume that the magnetic field is opened by the erupting CME we take the value of $B_{x0} \approx 0.04 < B_{z0} >$ resulting in small Alfvén speed in the $x-y$ plane, $V_{A,xy} = B_{x0}/\sqrt{4\pi\rho}$ compared to the total Alfvén speed $V_A = B/\sqrt{4\pi\rho}$, and the value of $V_0 = 5V_{A,xy}$. The value of the magnetic field in the observations is unknown. However, the results of the model are not sensitive to the magnitude of B_{z0}, and B_{x0} as long as $V_{A,xy} < V_0$. The boundary conditions are periodic in the x-direction, and open in the y-directions. The size of the modeled region in the y-direction is $10a$, and in the y-direction $\sim 5\pi a$ corresponding to the wavelength of the fastest growing mode (e.g., Miura & Pritchett 1982). The time is in units $\tau_A = a/V_{A,xy}$. The calculations are initialized with a small amplitude fundamental harmonic perturbation in velocity in the $x-y$ plane. The MHD equations are solved using the modified Lax-Wendroff method with 4th order artificial viscosity term on 260×260 grid. The resistivity does not play a significant role on the time scale of the evolution of KH instability that grows in few Alfvén times, and the Lundquist number is set to 10^4.

The results of the 2.5D MHD model of KH instability are shown in Figure 5 at $t = 17\tau_A$ in the nonlinear stage. The density structure and the corresponding velocity fundamental vortex generated by the KH instability are evident. The structure and the temporal evolution of the density corresponds to the traveling structures seen in the time sequence

of the SDO/AIA EUV emission in Figure 1 and in the corresponding animations of the data and the model. The model shows that later evolution leads to formation of smaller scale vortices, and the development of low density 'bubbles' in the high density region, similar to observational features (see the animations). Although, the present model is for simplified 2.5D configuration, it reproduces the main observational features, supporting the interpretation of the observations in terms of KH instability.

5. Discussion and Conclusions

We report the first EUV observations of the KH instability in the corona, which occurred along the interface between erupting and non-erupting material associated with the CME of April 8, 2010. The KH instability features are small (7000 km) and evolve on timescales of seconds, so it would be difficult to observe this phenomenon with an imager that has a lower resolution and cadence than SDO/AIA. The detailed formation and evolution of KH vortices is observed and analyzed. It was found that features along the velocity shear first exhibit the linear growth stage, but the instability quickly reaches nonlinear saturation (within tens of minutes), exhibiting the typical formation of KH vortices.

The growth and the evolution of the instability is compared to theoretical predictions in the linear stage, and to the results of 2.5D MHD model in the nonlinear stage, and good qualitative agreement is found. In particular, we find that the modeled vortices and associated density structures reach the saturated, nonlinear stage, and the dynamics of the features is qualitatively similar to the observed evolution in AIA images.

The detection of the KH instability in the solar corona further shows that KH instability is a ubiquitous process in natural fluids and plasmas that can play an important role in

energy transport in the corona on all scales. Theoretical studies find that KH instability is important in dissipation of free energy in shear flows and jets, and in the transition to turbulence. KH instability can also occur on small scales in solar coronal plasma in the presence of shear flows, leading to enhanced dissipation of waves and super-Alfvénic jets produced by impulsive events (such as flares) in the solar corona, and facilitate the heating of the solar coronal plasma.

REFERENCES

Berger, T. E., et al. 2010, ApJ, 716, 1288

Chandrasekhar, S. 1961, International Series of Monographs on Physics, Oxford: Clarendon

Farrugia, C. J., Sandholt, P. E., & Burlaga, L. F. 1994, J. Geophys. Res., 99, 19403

Frank, A., Jones, T. W., Ryu, D., & Gaalaas, J. B. 1996, ApJ, 460, 777

Hasegawa, H., Fujimoto, M., Phan, T.-D., Rème, H., Balogh, A., Dunlop, M. W., Hashimoto, C., & TanDokoro, R. 2004, Nature, 430, 755

Hermann von Helmholtz 1868, Monatsberichte der Kniglichen Preussische Akademie der Wissenschaften zu Berlin 23, 215

Heyvaerts, J., & Priest, E. R. 1983, A&A, 117, 220

Karpen, J. T., Dahlburg, R. B., & Davila, J. M. 1994, ApJ, 421, 372

Lord Kelvin (William Thomson) 1871, Phil. Mag. 42, 362

Kivelson, M. G., et al. 1998, J. Geophys. Res., 103, 19963

Lysak, R. L., & Song, Y. 1996, J. Geophys. Res., 101, 15411

Masters, A., et al. 2010, J. Geophys. Res., 115, 7225

Miura, A., & Pritchett, P. L. 1982, J. Geophys. Res., 87, 7431

Miura, A. 1984, J. Geophys. Res., 89, 801

Ofman, L., Chen, X. L., Morrison, P. J., & Steinolfson, R. S. 1991, Physics of Fluids B, 3, 1364

Ofman, L., Davila, J. M., & Steinolfson, R. S. 1994, Geophys. Res. Lett., 21, 2259

Ofman, L., & Sui, L. 2006, ApJ, 644, L149

Ofman, L., & Thompson, B. J. 2002, ApJ, 574, 440

Ryutova, M., Berger, T., Frank, Z., Tarbell, T., & Title, A. 2010, Sol. Phys., 170
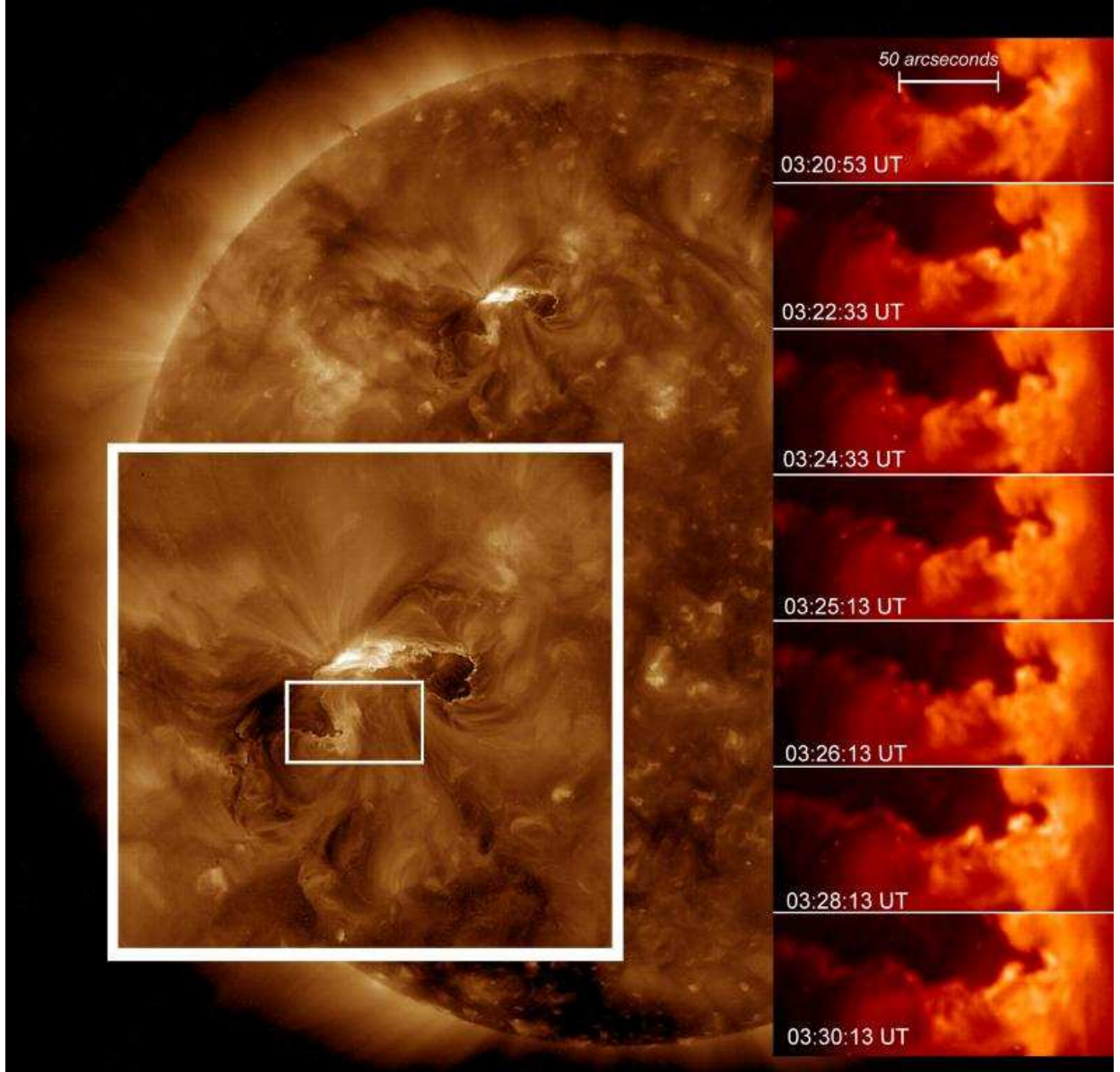
Slavin, J. A., et al. 2010, Science, 329, 665

Fig. 1.— The site of the CME eruption that begins around 02:34 UT on 8 April 2010 is shown in a full-disk 193Å image. The large white box is a zoomed-in view of the erupting structure, which exhibits dark regions of evacuated material as well as the flaring active region. The smaller box highlights the boundary between the dark region and the surrounding corona, which is where the KH vortices were observed. The sequence of frames on the right shows the temporal evolution of the vortices in 211Å images (see the accompanying animations of this event). We found that the KH features had the clearest visibility in the 211Å images.
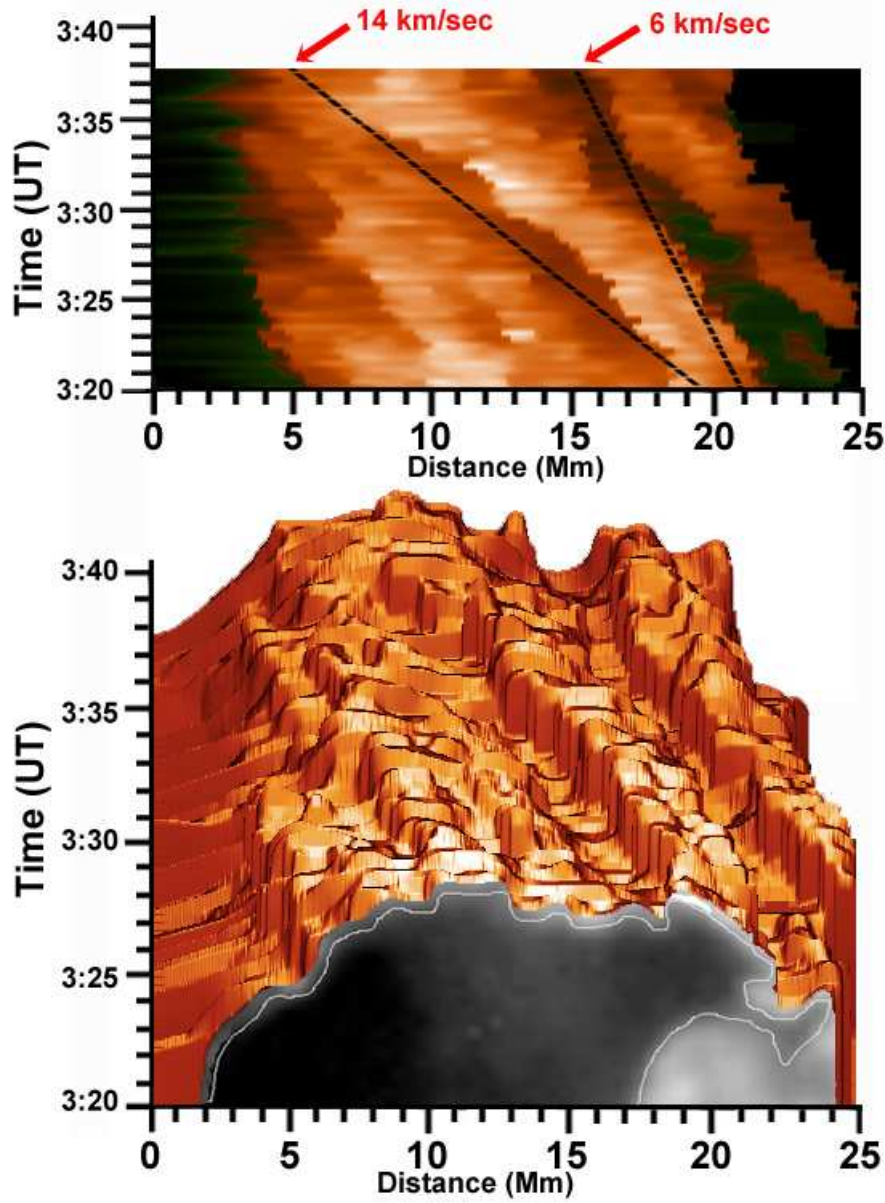
Fig. 2.— The lower image shows the motion along the interface between the evacuated (dark) corona and the surrounding non-eruptive region. The interface was outlined in 51 separate 211Å images, and the results are shown in contour plot of space vs. time. (Note that in this plot, the image coordinates are flipped vertically relative to the actual observations.) The top image is the projection of the lower plot onto the x-y plane. The slopes that correspond to motions of 6 km s^{-1} and 14 km s^{-1} are indicated with black dashed lines.
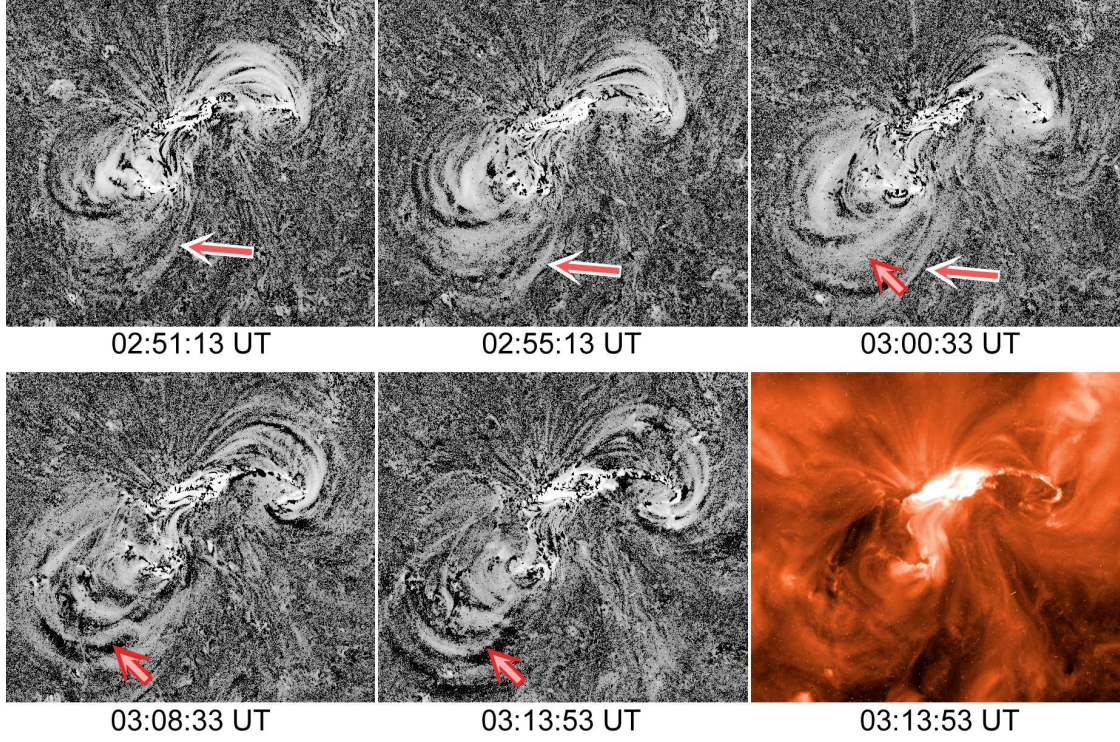
Fig. 3.— The first five panels are difference images that were created by subtracting consecutive pairs of 211Å images. The different types of arrow indicate the motions of two separate loops associated with the erupting CME shown in Figure 1. The lower right panel is a 211Å AIA image of the eruption region at 03:13:5UT, shown for context. The displacement motion of several different loops indicated that the motion near the arrows was around 20 km s^{-1}.
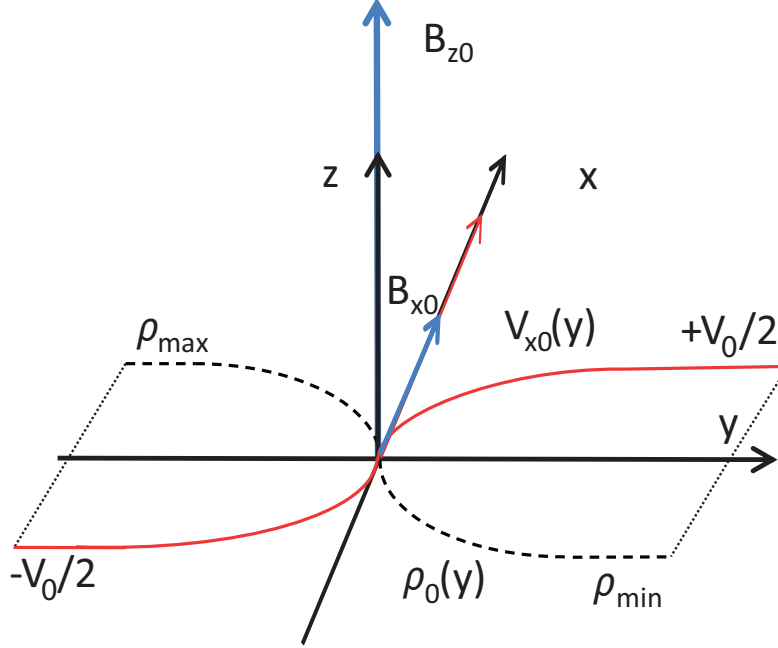
Fig. 4.— A sketch of the initial state used in 2.5D MHD model of the KH instability. The x-direction is parallel to the interface. The blue arrows show the magnetic field components (not to scale), where B_{z0} represents the strong radial magnetic field components associated with the erupting CME, and B_{x0} is the much weaker transverse field component. The red arrow shows the direction of the initial flow, the curves show schematically the variation of $V_{x0}(y)$ (red), and density $\rho_0(y)$ (dashes) across the interface.
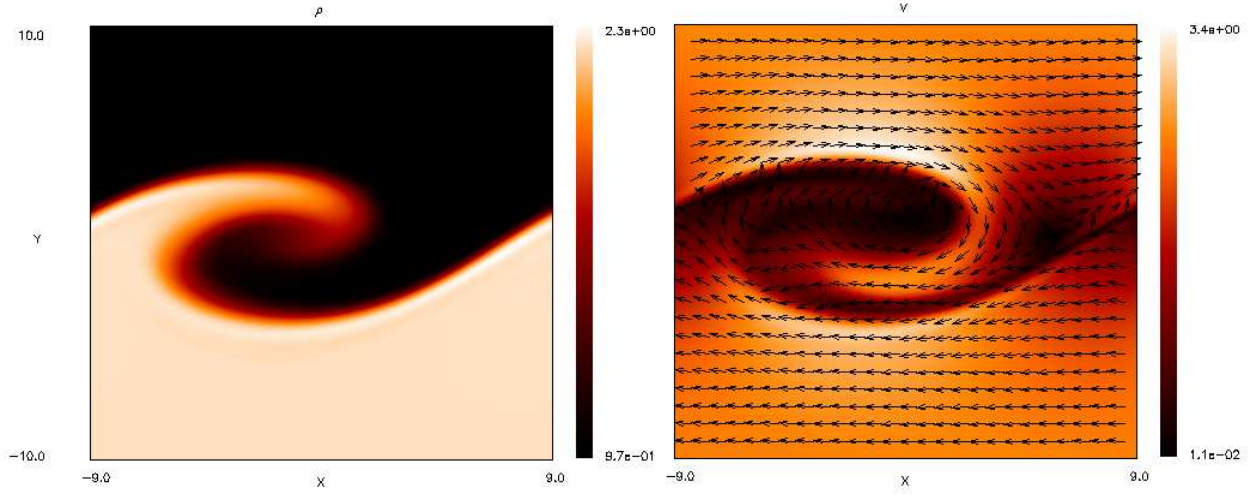
Fig. 5.— The density (left panel) and velocity (right panel) structures of the fully developed nonlinear KH instability at $t = 17\tau_A$ obtained with the 2.5D MHD model. The density is in units of ρ_{min}. The arrows show the direction of the flow, and the magnitude is in units of $V_{A,xy}$ (see text). The animation of the density and velocity evolution is enclosed in the electronic version of this paper.